OPEN ACCESS

Applied Physics Express 18, 062001 (2025) LETTER

https://doi.org/10.35848/1882-0786/addb1e

Coherent multiphoton photoemission spectroscopy of image-potential state on Ir (111) surface

Yu-Chan Tai[1,2], Chih-Wei Luo[2,3,4,5], Noriaki Takagi[6], Hiroshi Ishida[7], Chun-Liang Lin[2*], and Ryuichi Arafune[1*]

[1]Research Center for Materials Nanoarchitectonics (MANA), National Institute for Materials Science (NIMS), Tsukuba, Japan
[2]Dept. of Electrophysics, National Yang Ming Chiao Tung University (NYCU), Hsinchu City, Taiwan
[3]Center for Emergent Functional Matter Science, National Yang Ming Chiao Tung University (NYCU), Hsinchu, Taiwan
[4]Institute of Physics, National Yang Ming Chiao Tung University (NYCU), Hsinchu, Taiwan
[5]National Synchrotron Radiation Research Center, Hsinchu, Taiwan
[6]Graduate School of Human and Environmental Studies, Kyoto University, Kyoto, Japan
[7]College of Humanities and Sciences, Nihon University, Tokyo, Japan

*E-mail: clin@nycu.edu.tw; ARAFUNE.Ryuichi@nims.go.jp

Received April 18, 2025; revised May 16, 2025; accepted May 19, 2025; published online June 6, 2025

Multiphoton photoemission provides a means to investigate unoccupied electronic states via nonlinear light-matter interactions. In this work, we employ five-photon photoemission spectroscopy to identify, for the first time, the image-potential state (IPS) on the Ir(111) surface. Distinct from commonly studied noble metals such as Cu and Ag, the Ir(111) electronic structure leads to a strong sensitivity to excitation energy: a reduction from 1.57 eV to 1.49 eV significantly diminishes the signal. The theoretical analysis attributes this effect to the *d*-band proximity to the Fermi level, which influences the initial-state population and transition probabilities governing the multiphoton excitation pathways.

Laser-based photoemission spectroscopy has become essential in solid-state physics research, enabling the high-precision study of electronic states and dynamics. Many phenomena that cannot be observed using conventional light sources, such as discharge lamps or synchrotron radiation, have been successfully studied using laser-based approaches.[1–8] Among these, coherent nonlinear photoemission spectroscopy with ultrafast laser pulses has proven to be a powerful method for probing unoccupied electronic states, providing insights into excited-state dynamics and band structures.

Time-resolved two-photon photoemission (2PPE) spectroscopy has significantly advanced our understanding of electron dynamics at solid surfaces, leading to numerous studies in this field.[1,2,9,10] However, multiphoton photoemission (mPPE, $m \geqslant 3$), termed higher-order nonlinear photoemission, or above-threshold photoemission,[6,11] which includes both coherent and incoherent processes, remain underexplored. The complex relationship between the electronic band structures and multiphoton excitation pathways necessitates further experimental investigations. mPPE spectroscopy is a powerful tool for probing the relationship between the electronic band structure and light–matter interaction in the nonlinear regime.

In this letter, we report the first experimental observation of the image-potential state (IPS) on Ir(111) using coherent five-photon photoemission (5PPE) spectroscopy. The image-potential state is one of the important classes of unoccupied states. They are quantized electronic states arising from the Coulombic attraction between an electron and its induced image charge at a metallic surface. They are localized outside the surface and serve as model systems for electron-surface interactions and quantum confinement. Their properties strongly depend on surface screening, electronic structures, and dielectric responses, making them valuable probes of surface electronic properties. While IPSs have been well studied via 2PPE on noble metals like Ag[12–15] and Cu,[14,16–18] these studies typically employ harmonic generation to reach the required photon energy. In contrast, our use of 5PPE highlights the role of nonlinear excitation pathways and their sensitivity to band structure. Furthermore, to our knowledge, no reports have been made on the clean Ir(111) surface. These results pave the way for further studies into light–matter interaction in nonlinear regimes.

The experiment was performed in a UHV chamber (2×10^{-10} Torr) with a Ti:sapphire oscillator (80 MHz) generating near-IR pulses at $\lambda = 790$ nm and 833 nm ($\hbar\omega = 1.57$ eV and 1.49 eV) with laser powers of 1.1 W and 1.2 W, respectively. The pulses (120 fs duration, 100 μm spot size) were focused onto the Ir sample. mPPE spectra were measured in normal emission with the p-polarized light incident at 45°. The Ir(111) surface was cleaned by sputtering and annealing, and its quality was confirmed by low-energy electron diffraction and mPPE spectra. Photoelectrons were detected with a hemispherical analyzer (Phoibos 100) and a 2D detector, yielding $E_f(k_{\|})$ spectra with 20 meV energy resolution.

No signs of sample damage or signal distortion due to space-charge effects[19,20] were observed throughout the experiment, and the corresponding stability was confirmed by the reproducibility of the multiphoton photoemission spectra, even after prolonged irradiation of the same sample spot over several hours.

We performed theoretical calculations using the computer code[21] within the density functional theory (DFT) framework, combined with the embedded Green's function technique[22] and the full-potential linearized augmented plane-wave method[23]. This approach has been used to calculate the electronic structure of semi-infinite Ir(001) and Au(001) surfaces[24–26]. We used the DFT-LDA exchange-correlation energy functional since DFT-GGA underestimates work functions of 5*d* metals typically by a few tenths of eV. Furthermore, in order to be able to reproduce IPSs, the planar average of the short-range DFT one-electron potential,

$\bar{V}_{\mathrm{eff}}(z)$ with z being the surface normal coordinate, is admixed gradually with a model image-potential by using an interpolation function proposed by Nekovee and Inglesfield [27] as

$$V(z) = [1 - \rho(z)]\,\bar{V}_{\mathrm{eff}}(z) + \rho(z)\left[E_{\mathrm{vac}} - \frac{1}{4(z - z_{\mathrm{im}})}\right], \quad (1)$$

where E_{vac} denotes the vacuum level, and $\rho(z)$ varies smoothly from 0 at $z = z_{\mathrm{im}}$ (the image plane) to 1 at $z = z_b$ (the embedding surface on the vacuum side). The effects of the asymptotic Coulomb potential beyond z_b are incorporated by the embedding potential acting on $z = z_b$. The image plane ($z_{\mathrm{im}} = 1.58$ Å) position is determined by the center of mass of the charge density induced by a weak static electric field, with the topmost Ir atom position defined as $z = 0$.[27–30]

Figure 1(a) shows the mPPE spectra of the clean Ir(111) surface at the $\bar{\Gamma}$ point. These spectra were measured using the 1.57 and 1.49 eV laser photons, respectively. The work function was determined to be 5.83 eV from the lower cutoff energy, consistent with previously reported values.[31] These spectra result from 4PPE and 5PPE processes, as determined by considering the photon energy and the measured work function. The solid curves in Fig. 1(a) are the fitting curves, which determine the peak positions and intensities of the spectra. The peak positions are 6.68 and 6.60 eV excited by 1.57 and 1.49 eV photons, respectively. The photoemission intensity excited by 1.57 eV photons is stronger than that of 1.49 eV photons. At the $\bar{\Gamma}$ point, the intensity of the peak excited by 1.57 eV photons, determined from the fitting, is 0.28 cps, while that of 1.49 eV photons is 0.08 cps. This intensity difference arises from the difference in the density of states (DOS) of the initial states corresponding to the two photon energies, as will be discussed later.

To understand the origin of the peaks observed in Fig. 1(a), we have examined their assignment based on spectral and momentum-resolved characteristics. The band dispersion is evaluated from the momentum-resolved mPPE spectra shown in Fig. 1(b). The parabolic shape of the band yields an effective mass of $(1.1 \pm 0.1)m_o$ (where m_o is the free-electron mass), showing a characteristic of IPS. However, it should be noted that the IPS of clean Ir(111) has not been determined experimentally. A careful analysis is required for the definitive assignment. In order to firmly assign the observed peak to IPS, we consider the possible excitation pathways in the mPPE process. The difference between the final-state energies (6.68 and 6.60 eV) matches the difference in photon energies (1.57 and 1.49 eV), suggesting a common intermediate state located at 5.11 eV above the Fermi level. This value indicates that four photons were absorbed for excitation from the initial occupied state to the intermediate state, followed by the additional photon causing an electron to emit into vacuum, as shown in Fig. 1(c). From the energy position, the effective mass, and the band shape, we conclude that this peak originates from IPS.

We further compare the energy position of experimental observation with theoretical predictions to validate the IPS assignment. The observed IPS ($n = 1$) is at 0.73 eV below the vacuum level at the $\bar{\Gamma}$ point. Figure 2 shows the intensity of momentum-resolved DOS calculated in the first layer of the Ir(111) surface, consistent with prior findings[32]. The bright region corresponds to a projected bulk band gap. In contrast, the dark-gray regions on the higher-energy sides are projected bulk bands of Ir, except for the parabolic region $E - E_V \geqslant \hbar^2k^2/2m_o$, which corresponds to the projection of the energy continuum of the semi-infinite vacuum. The series of IPSs ($n = 1, 2, \ldots$) appeared inside the projected band gap at the $\bar{\Gamma}$ point, exhibiting free-electron-like parabolic energy dispersions with k. We obtained 5.88 and 0.63 eV as the work function and the binding energy referred to the vacuum level at the $\bar{\Gamma}$ point of the $n = 1$ IPS, respectively. These values agree well with our experimental values. These calculation results further support our assignment.

On most (111) surfaces of FCC metals, an energy gap exists around the vacuum level and $\bar{\Gamma}$ point, which is a requisite for IPSs. While image-potential-included *ab-initio* calculated

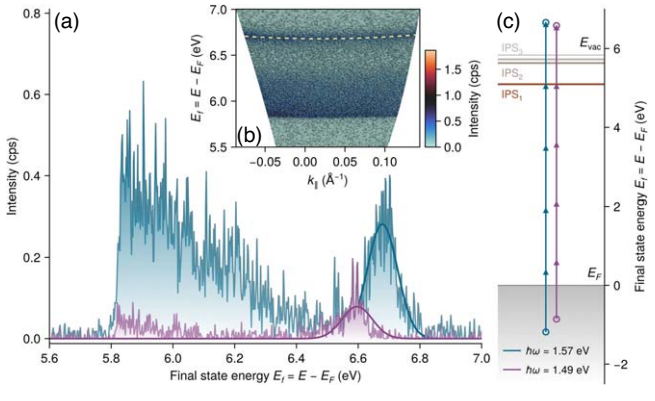

Fig. 1. (a) The mPPE spectra of the clean Ir(111) surface excited with 1.57 and 1.49 eV photons at the $\bar{\Gamma}$ point. Solid curves are peak-fitting (Lorentzian) results to evaluate the peak position and intensity. (b) The momentum resolved mPPE spectra excited with $\hbar\omega = 1.57$ eV photons. A color bar indicates photoemission intensity, while the dashed parabola highlights band dispersion. (c) Schematic illustration of the mPPE pathway leading to the first IPS and subsequent photoemission at the Γ point of the Ir(111) surface. The three horizontal brown lines show the calculated IPSs (see Fig. 3 for wave functions and binding energies). Under four-photon absorption from an initial state at the Γ point, electrons are excited to the first IPS before a fifth photon emits them into vacuum.

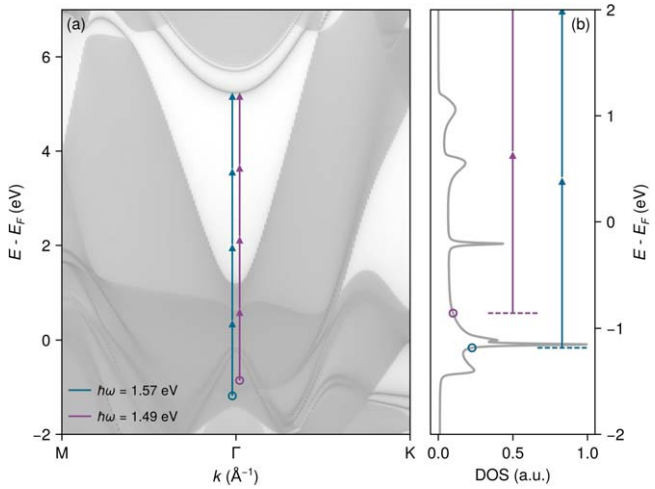

Fig. 2. (a) A log-intensity map of first-layer DOS, $\rho(k, \epsilon)$, for the Ir(111) surface electronic structure along the M-Γ-K direction. The blue and purple arrows highlight the four-photon photoexcitation pathways for the 1.57 eV and 1.49 eV conditions, respectively, illustrating how electrons transition from initial states below the Fermi level to populate the IPS. The blue and purple circles mark each excitation energy's initial state. (b) The Γ point DOS, averaged over the topmost five layers and incorporating an imaginary energy $\gamma = 10$ meV, highlights the initial states involved in the multiphoton excitation processes at the two photon energies.

semi-infinite Ir(111) surface electronic structure provides detailed insight, it is also informative to consider established analytical models that describe IPS formation [1,15,33–36]. The analytical model often makes it easier to understand how the results depend on various parameters intuitively. Chulkov *et al.*[35] developed a one-dimensional pseudo-potential model to predict the binding energies of IPSs on such metal surfaces. The model potential is represented by the following formula:

$$V(z) = \begin{cases} -A_{10} + A_1 \cos(2\pi z/a_m), & z \leqslant 0 \\ -A_{20} + A_2 \cos(\beta z), & 0 < z \leqslant z_1 \\ -A_3\, e^{-\alpha(z-z_1)}, & z_1 < z \leqslant z_{\mathrm{im}} \\ \dfrac{e^{-\lambda(z-z_{\mathrm{im}})} - 1}{4\,(z - z_{\mathrm{im}})}, & z_{\mathrm{im}} < z \end{cases} \quad (2)$$

The potential $V(z)$ and its derivative must be continuous at the matching points z_1 and z_{im}, leaving four independent parameters (A_1, A_{10}, A_2, β) to describe the potential profile: A_1 and A_{10} govern the periodic potential below the surface, while A_2 and β control the smooth transition to the asymptotic image-potential. Armbrust *et al.*[36] estimated the parameters from the experimental results on the IPSs of the graphene-covered Ir(111), as no such data were available for clean Ir(111). Here, we examine the validity of the parameters they estimated by using our experimental results. Figure 3 shows the wave functions of the first three IPSs with the model potential. The binding energies of them at the $\bar{\Gamma}$ point are represented by the brown horizontal bars in Fig. 1(c). The excited electron in the $n = 1$ IPS is most likely localized at 3.25 Å from the Ir(111) surface. The binding energy of the $n = 1$ IPS is 5.094 eV above the Fermi level (−0.741 eV concerning the vacuum level), which is very close to the experimental value.

Having established the nature and energy of the IPS, we now assess the efficiency of the multiphoton excitation pathways that lead to its population. As described above, the IPS peak intensity under 1.57 eV excitation (0.28 cps) is notably higher than that under 1.49 eV excitation (0.08 cps), as determined from the peak fittings in Fig. 1(a). We have carefully aligned the laser and sample positions to the analyzer to ensure the two spectra are directly comparable. (The mPPE intensity is more susceptible to the laser fluence and the sample position than in the 1PPE experiments; such high sensitivity enables precise alignment.) To model the intensity, we adopt the general power-law dependence $I = c \cdot P^m$, where P is the excitation power and $m = 5$ corresponds to the order of the nonlinear process. We further assume that the prefactor c reflects initial-state properties, mainly the local DOS at the excitation energy. This approach parallels the standard ARPES intensity expression $I \propto |M|^2 \rho(\epsilon)$, where $\rho(\epsilon)$ is the initial-state DOS and M the transition matrix element. Assuming the matrix elements for the excitation from the d-band to the IPS are comparable for both photon energies, the intensity ratio can be primarily attributed to differences in the initial-state DOS.

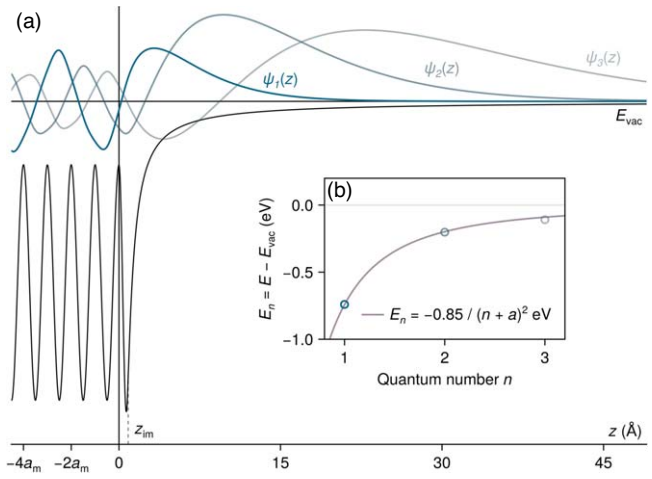

Fig. 3. (a) A one-dimensional pseudo-potential model was used to determine the binding energies of IPSs at the Γ point of the Ir(111) surface. The corresponding eigenfunctions for the first three IPSs are shown, illustrating that the first IPS wavefunction ($z > 0$) localizes the image-potential charge about 3.25 Å from the Ir(111) surface. (b) The calculated binding energies of these three IPSs, approximated using the Rydberg formula $E_n = -0.85/(n + a)^2$ with a 7.03×10^{-2} quantum defect.

To support this interpretation, in Fig. 2(b), we show our DFT-calculated DOS averaged over the topmost five layers. To account for spectral broadening due to the lifetime effects and the finite energy resolution, the DOS was calculated with an imaginary energy $\gamma = 10$ meV. Compared with the previous ARPES measurement at the $\bar{\Gamma}$ point [37], the Ir d-band exhibits a pronounced DOS peak near −1.15 eV. The 1.57 eV excitation accesses an initial state of −1.18 eV, which is very close to this high-DOS region, enhancing the 5PPE transition probability. In contrast, reducing the photon energy to 1.49 eV shifts the initial state upward by approximately 320 meV, distancing it from the d-band peak and significantly reducing the local DOS available for excitation. The qualitative agreement with published ARPES data and the observed intensity ratio confirms that the enhanced 5PPE signal under 1.57 eV excitation can be attributed to its favorable alignment with a high-DOS region of the Ir d-band. These observations highlight how subtle changes in excitation energy significantly alter the photoemission signal through their influence on the initial-state DOS. While the present study employs two photon energies, which we find sufficient to support our main conclusions, systematic photon-energy-dependent measurements, in combination with ARPES, would enable us to more precisely analyze how the band structure influences the multiphoton excitation process.

Identifying higher-order ($n \geqslant 2$) IPSs and observing higher-order photoemission processes ($m \geqslant 6$), even for $n = 1$ IPS, remains challenging. The above theoretical calculation shows that 1.57 and 1.49 eV photons have sufficient energy to excite the occupied electron to the higher-order IPSs via the 5PPE process. However, the transition to the higher-order IPSs is less likely compared to the $n = 1$ IPS because their wave functions are spatially farther from the solid surface, as shown in Fig. 3. For example, the IPSs of Cu(001) measured by using 2PPE, the intensity of 2PPE peak is approximately proportional to n^{-2} [1]. Although this n^{-2} scaling is derived from 2PPE, it provides a reasonable first-order estimate for the attenuation trend in higher-order processes. This attenuation of intensity poses challenges, especially in detecting higher-order states. The 6PPE process provides a possibility to overcome this challenge. In this scenario, four photons are used to excite the electron from the occupied states to the IPS, and two photons are used to excite it to emit into vacuum. Reutzel *et al.* have succeeded in detecting the 6PPE spectrum of the Cu(111), Ag(111), and Au(111) [6]. In their

experiments, the initial occupied state is a surface state with high DOS. They observed $m = 4$ to 6 photon photoemission spectra of the surface state and showed that the 6PPE intensity is at least ten times weaker than the 5PPE intensity. We suppose that the ratio of the 6PPE intensity to the 5PPE intensity of the IPS is also attenuated in the same order. Such weak 6PPE signals fall below our detection threshold, making them difficult to observe. Note that the 6PPE spectra of the IPSs have not been observed in the literature. It would be interesting to detect this 6PPE, 3PPE by using second-harmonic generated photons or other combinations of the photon energies[38,39] from the perspective of the physics of multiphoton excitation on solid surfaces.

In summary, we have measured 5PPE spectra of the clean Ir(111) surface and determined the energy position of the first IPS. Furthermore, our mPPE results disclose how the surface electronic structure and DOS govern multiphoton excitation pathways, eventually dictating the observed spectra. These results exemplify the applicability of mPPE spectroscopy for probing initial, intermediate, and final states in complex excitation processes and enrich our understanding of how IPSs in high-work-function transition metals are populated via multiphoton excitation. Future investigations may focus on time-resolved studies to measure IPS's lifetime or extend this approach to other metallic surfaces with varying screening properties, expanding our understanding of non-linear photoemission dynamics at metal-vacuum interfaces.

Acknowledgments This work was financially supported by JSPS KAKENHI (Grant No. 22H0196) and the World Premier International Research Center Initiative (WPI) on Materials Nanoarchitectonics, MEXT, Japan. The National Science and Technology Council (NSTC) of Taiwan supported this study, in part, under the contracts of NSTC 113-2119-M-A49-001-MBK, 113-2112-M-A49-020-MY3, 114-2923-M-A49-001-MY2, 113-2628-M-A49-006-MY3, 112-2923-M-A49-001-MY2, and NSTC T-Star Center Project, Future Semiconductor Technology Research Center, under NSTC 114-2634-F-A49-001-.

ORCID iDs Yu-Chan Tai https://orcid.org/0009-0000-3010-9283
Chih-Wei Luo https://orcid.org/0000-0002-6453-7435
Noriaki Takagi https://orcid.org/0000-0002-0799-9772
Hiroshi Ishida https://orcid.org/0000-0003-2080-1561
Chun-Liang Lin https://orcid.org/0000-0001-8781-3650
Ryuichi Arafune https://orcid.org/0000-0003-4371-6116

1) U. Höfer, I. L. Shumay, C. Reuß, U. Thomann, W. Wallauer, and T. Fauster, Science **277**, 1480 (1997).
2) H. Petek, M. J. Weida, H. Nagano, and S. Ogawa, Science **288**, 1402 (2000).
3) T. Kiss et al., Phys. Rev. Lett. **94**, 057001 (2005).
4) R. Arafune, K. Hayashi, S. Ueda, Y. Uehara, and S. Ushioda, Phys. Rev. Lett. **95**, 207601 (2005).
5) J. Reimann et al., Nature **562**, 396 (2018).
6) M. Reutzel, A. Li, and H. Petek, Phys. Rev. B **101**, 075409 (2020).
7) M. browski, Y. Dai, and H. Petek, Chem. Rev. **120**, 6247 (2020).
8) S. Ito et al., Nature **616**, 696 (2023).
9) J. Güdde, M. Rohleder, T. Meier, S. W. Koch, and U. Höfer, Science **318**, 1287 (2007).
10) N. Armbrust, J. Güdde, P. Jakob, and U. Höfer, Phys. Rev. Lett. **108**, 056801 (2012).
11) F. Banfi, C. Giannetti, G. Ferrini, G. Galimberti, S. Pagliara, D. Fausti, and F. Parmigiani, Phys. Rev. Lett. **94**, 037601 (2005).
12) R. W. Schoenlein, J. G. Fujimoto, G. L. Eesley, and T. W. Capehart, Phys. Rev. B **43**, 4688 (1991).
13) R. Lingle, N. H. Ge, R. Jordan, J. McNeill, and C. Harris, Chem. Phys. **205**, 191 (1996).
14) A. Damm, K. Schubert, J. Güdde, and U. Höfer, Phys. Rev. B **80**, 205425 (2009).
15) M. Marks, C. H. Schwalb, K. Schubert, J. Güdde, and U. Höfer, Phys. Rev. B **84**, 245402 (2011).
16) T. Hertel, E. Knoesel, M. Wolf, and G. Ertl, Phys. Rev. Lett. **76**, 535 (1996).
17) M. Wolf, E. Knoesel, and T. Hertel, Phys. Rev. B **54**, R5295 (1996).
18) M. Weinelt, J. Phys.: Condens. Matter **14**, R1099 (2002).
19) S. Passlack, S. Mathias, O. Andreyev, D. Mittnacht, M. Aeschlimann, and M. Bauer, J. Appl. Phys. **100**, 024912 (2006).
20) J. Graf, S. Hellmann, C. Jozwiak, C. L. Smallwood, Z. Hussain, R. A. Kaindl, L. Kipp, K. Rossnagel, and A. Lanzara, J. Appl. Phys. **107**, 014912 (2010).
21) H. Ishida, Phys. Rev. B **63**, 165409 (2001).
22) J. E. Inglesfield, J. Phys. C: Solid State Phys. **14**, 3795 (1981).
23) D. J. Singh and L. Nordström, 2006)*Planewaves, Pseudopotentials, and the LAPW Method 2nd ed* (Springer, New York, NY).
24) H. Ishida, Phys. Rev. B **90**, 235422 (2014).
25) T. Nakazawa, N. Takagi, M. Kawai, H. Ishida, and R. Arafune, Phys. Rev. B **94**, 115412 (2016).
26) H. Ishida, Surf. Sci. **744**, 122472 (2024).
27) M. Nekovee and J. Inglesfield, Prog. Surf. Sci. **50**, 149 (1995).
28) N. D. Lang and W. Kohn, Phys. Rev. B **7**, 3541 (1973).
29) N. D. Lang, Phys. Rev. Lett. **46**, 842 (1981).
30) R. O. Jones, P. J. Jennings, and O. Jepsen, Phys. Rev. B **29**, 6474 (1984).
31) D. Niesner, F. Th, J. I. Dadap, N. Zaki, K. R. Knox, P. C. Yeh, R. Bhandari, R. M. Osgood, M. Petrović, and M. Kralj, Phys. Rev. B **85**, 081402 (2012).
32) A. Varykhalov, D. Marchenko, M. R. Scholz, E. D. L. Rienks, T. K. Kim, G. Bihlmayer, J. Sánchez-Barriga, and O. Rader, Phys. Rev. Lett. **108**, 066804 (2012).
33) K. Giesen, F. Hage, F. J. Himpsel, H. J. Riess, and W. Steinmann, Phys. Rev. B **35**, 971 (1987).
34) T. Fauster, Appl. Phys. A **59**, 639 (1994).
35) E. Chulkov, V. Silkin, and P. Echenique, Surf. Sci. **437**, 330 (1999).
36) N. Armbrust, J. Güdde, and U. Höfer, New J. Phys. **17**, 103043 (2015).
37) I. Pletikosić, M. Kralj, D. Šokčević, R. Brako, P. Lazić, and P. Pervan, J. Phys.: Condens. Matter **22**, 135006 (2010).
38) S. Link, H. A. Dürr, G. Bihlmayer, S. Blügel, W. Eberhardt, E. V. Chulkov, V. M. Silkin, and P. M. Echenique, Phys. Rev. B **63**, 115420 (2001).
39) U. Thomann, C. Reuß, T. Fauster, F. Passek, and M. Donath, Phys. Rev. B **61**, 16163 (2000).